



Original Paper

A New Approach to Optimize Ultimate Geometry of Open Pit Mines with Variable Overall Slope Angles

Firdevs Kübra Altuntov¹ and Mustafa Erkayaoglu^{1,2}

Received 15 March 2021; accepted 19 June 2021

Published online: 3 July 2021

The optimization method for determining open pit limit is important, as it is crucial to achieve the most profitable outcome from the limited amount of reserves available. However, importance must be also given to geotechnical aspects to ensure that safety requirements are met. Thus, overall slope angle (OSAs) must be incorporated in the optimization process. In the conventional methods, there were problems in incorporating various OSAs, or they were included in the pit design after the completion of the optimization procedure. To include variable OSAs in the optimization, cone-based method is still considered as one of the most suitable approaches. To apply this method, a new mathematical model incorporating various OSAs into the ultimate pit problem through mixed integer programming (MIP) and simulated annealing is proposed. Four different cases of change in OSAs in the pit were included in the algorithm. The proposed method was verified by applying it to five different cases, and the OSA was achieved with a considerably low difference of 0°–2° while optimizing the ultimate pit. The comparison between the introduced algorithm and the Lerchs–Grossman algorithm indicated that an improvement within a range of 8–20% can be achieved.

KEY WORDS: Pit optimization, Mixed integer programming, Ultimate pit limit, Open pit mining, Simulated annealing.

INTRODUCTION

According to the guidelines published by Canadian Institute of Mining (CIM) on resource and reserve estimation (CIM, 2019), for mineral resources that can be extracted by open pit mining methods, forecasts for the extraction must include not only the economical limit but also technical necessities (such as slope angles). With these limitations, an enquiry is carried out to find out whether the mineral resource can be qualified as a reserve. The optimization for the qualification of a mineral

resource as a reserve is performed to determine the ultimate pit limit. In most of the approaches, nested pits are generated from the smallest to the largest pit by changing the economic parameters to form pushbacks within the final pit limit. Then, annual production schedule is planned from these pushbacks (Osanloo et al., 2008). In other approaches, blocks are directly scheduled to form the final pit contour (Campos et al., 2018; Farmer & Dimitrakopoulos, 2018; Johnson, 1968; Souza et al., 2018). Researchers also investigated the applicability of machine learning algorithms to optimize the integration between mining and mineral processing by using mine planning block models (Li et al., 2020). The aim of this article was to generate an ultimate pit limit for variable overall slope angles

¹Mining Engineering Department, Middle East Technical University, Ankara, Turkey.

²To whom correspondence should be addressed; e-mail: emustafa@metu.edu.tr

(OSAs) that can be modified for different azimuth and depth values.

Researchers developed different algorithms to solve optimization-related problems in mining. Some exact, heuristic, metaheuristic, and stochastic methods such as dynamic programming, graph theory, moving cone method, genetic algorithm, artificial neural network, imperialist competitive algorithm, and Markov chain process have been proposed for the ultimate pit problem. The first dynamic programming to solve the ultimate pit limit problem was presented by Lerchs and Grossmann (1965). Other researchers attempted to improve it for 3D applications and for smoothing the pit geometry (Johnson & Sharp, 1971; Koenigsberg, 1982; Shenggui & Starfield, 1985; Wilke & Wright, 1984). The first graph theory algorithm for 3D ultimate pit limit developed by Lerchs and Grossmann (1965) was revisited by other researchers mainly focusing on reducing solution time (Barnes & Johnson, 1982; Chen, 1976; Huttagosol, 1988; Lipkewich & Borgman, 1969; Rychkun & Chen, 1979; Stuart, 1992; Zhao & Kim, 1992). Johnson (1968) demonstrated the relationship between the ultimate pit limit problem and the maximum flow. Picard (1976) mathematically demonstrated that the Lerchs and Grossmann (LG) algorithm was equivalent to finding a maximum flow on a graph. Hochbaum and Chen (2000) conducted efficiency tests to determine whether the maximum flow algorithm is the most effective way for resolving this type of problem. According to the results provided by Hochbaum and Chen (2000), push-relabel algorithm is considered to be one of the most promising algorithms. Hochbaum (2008) proposed another method called pseudo-flow algorithm in order to solve maximum flow problem. It was found that pseudo-flow algorithm is faster than Lerchs and Grossmann's algorithm (Deutsch et al., 2015). It has been used in many mining software programs such as Deswik and Geovia Whittle (Bai et al., 2017; Poniewierski, 2018).

Heuristic and metaheuristic methods such as floating cone, genetic algorithm and artificial neural network were introduced by researchers to deal with the drawbacks of the conventional methods used to determine the ultimate pit limit. The first floating cone method was proposed by Pana (1965), and variations of this method were proposed by various researchers (Elahi et al., 2011; Khalokakaie, 2006; Wright, 1999). In spite of its ease of application and comparably fast solution, this technique does not

necessarily provide optimum results. Milani (2016) proposed a non-standard genetic algorithm with zooming strategy for 2D and 3D pit layouts. Achireko (1998) proposed an algorithm in which artificial neural network is used to include stochastic properties of ore grade and commodity prices in pit limit optimization. According to Sayadi et al. (2011), the algorithm requires modifications for 3D pit layouts. Thus, they proposed a new 3D pit optimization algorithm, in which artificial neural network is used to find the ultimate pit limit. Javadzadeh et al. (2019) presented a new algorithm to solve ultimate pit limit problem by using imperialist competitive algorithm; it is based on the social-political process of creating an empire and enabled comparatively higher convergence speed to reach the ultimate pit in their application. Jalali et al. (2006) applied Markov chain process, which depends on a defined probability density function (pdf), to the ultimate pit limit problem; they stated that the probability of mining each block is determined to construct the optimum pit limits. The methods about incorporating slope angles in the optimization can be classified as methods depending on precedence relation between blocks and cone template method (Khalokakaie, 1999). Generally, in conventional methods, precedence of extraction in forms of patterns such as 1-5 and 1-9 relation between blocks are used. In 1-5/1-9 pattern, 5/9 overlying blocks above the base block are extracted first to remove the base block. The main disadvantage of these methods is that desired slope angle cannot be formed in every cross section, and slope angle depends on block dimensions.

Instead of precedence pattern, to incorporate slope angles, the cone template was proposed by researchers (Giannini, 1990; Lipkewich & Borgman, 1969; Zhao & Kim, 1992). In cone-based methods, blocks in the cone template are considered as selected. Lipkewich and Borgman (1969) proposed a pattern to approximate a cone template. In this pattern, eight blocks from two levels above the base block and five blocks from one level above the base block are removed before the base block is extracted under 45° slope restriction for a cubic block model. This approach is also insufficient to create the desired variable slope angles due to the similar reasons as in the approaches of precedence relation. In the approaches proposed by Chen (1976), Zhao and Kim (1992) and Dowd and Onur (1993), the cone template was used for variable slope angles, but only a single-slope angle was defined. Khalokakaie (1999) published a study in which variable slopes were

incorporated in LG algorithm, whereby the orebody was divided into four principle directions in which different slopes were formed by using the equation of an ellipse geometry. In these methods, linear interpolation and limited number of directions for the slopes causes non-smooth and impractical pit outlines. Because of this reason, Sattarvand and Shisvan (2012) proposed spline interpolation for modeling variable slope angles. Spline interpolation methods such as cubic, quadratic and cardinal were tested, and it was concluded that cubic spline interpolation creates more accurate pit outlines. Any number of slopes in any azimuth can be created with cubic spline interpolation. According to Gilani and Sattarvand (2015), cubic spline interpolation also performs well with multiple number of azimuths.

Meyer (1969) was the first to formulate the problem of ultimate pit contours as a problem of linear programming (LP). However, linear and mixed integer programming (MIP) are mostly used in production planning (Askari-Nasab et al., 2011; Blom et al., 2017, 2018; Fu et al., 2019; Kumral, 2012; L'Heureux et al., 2013; Ramazan & Dimitrakopoulos, 2004), which includes the optimum transition from open pit to underground mining methods (Soltani Khaboushan & Osanloo, 2020). Simulated annealing (SA) is also widely applied to the problem of production planning by many researchers (Albor Consuegra & Dimitrakopoulos, 2009; Kumral, 2013; Kumral & Dowd, 2004; Mousavi et al., 2016) and as part of the optimization of mining boundaries for lateritic metal deposits (Dagasan et al., 2019). In this paper, the SA was used in a different context to determine the pit bottom as the starting location for the optimization algorithm, which in turn also enables a decrease in the solution time.

The main template of SA algorithm was designed by Metropolis et al. (1953). SA was first utilized for optimization by Kirkpatrick et al. (1983) and Cerny (1985). In the 1980s, SA was used for combinatorial optimization but later continuous optimization problems were also solved with SA (Dekkers & Aarts, 1991; Locatelli, 2000; Ozdamar & Demirhan, 2000). SA was inspired by the annealing process where a material is heated and then gradually cooled down to achieve a strong crystalline structure. Unsuitable initial temperature and/or rapid cooling can result in flawed crystalline structure. Thus, temperature is slowly decreased to obtain strong crystals. As the temperature reaches to a suitable temperature level, the equilibrium state is

reached. SA algorithm simulates this cooling process. The equilibrium state and the energy state of the structure correspond to the optimum solution and the objective function value, respectively (Talbi, 2009).

In the algorithm proposed in this article, the cone-based method was utilized to incorporate multiple OSAs in the optimization. However, the shape of the pit template is not a cone because benches are formed and/or OSA is not constant when forming the pit contour during the design stage. The pit contour can be constructed for four situations where OSA is constant or variable with respect to depth, or azimuth, or with both depth and azimuth in the algorithm. Cubic spline interpolation was used in two cases where OSA varies with respect to azimuth. With this interpolation, the points in the horizontal plane of the pit contour were interpolated. Incorporating slope angles can provide more practical pit outlines (Sattarvand & Shisvan, 2012); therefore, the algorithm creating steeper slopes may result in more profitable pits as the objective function value increases as the slope angle increases (Chaves et al., 2020; Madowe, 2016; Malli et al., 2015). The optimization algorithm introduced in this study was carried out with MIP and SA, supported by a geotechnical study that defined the OSAs required for safe production. Further information for geotechnical analysis can be found in the study carried out by Parra et al. (2018).

ULTIMATE PIT LIMIT OPTIMIZATION ALGORITHM

In the proposed algorithm, the optimum pit limit was determined by ensuring that preset OSAs are obtained considering the geometrical parameters of the pit template, such as bench height and bench slope. The solution obtained from the algorithm gives depth of the pit, maximum radius of the pit, bench width, and total economic value of blocks. Input data required for the algorithm are bench height, bench slope, and parameters used for calculating economic value of blocks. In the algorithm, firstly, the maximum number of benches is determined followed by generating the mathematical model starting from the first level of bench and optimization carried out for all levels. The procedure is repeated until reaching the maximum number of benches and finally selecting the bench levels,

which provide the maximum result of economic value.

The incorporation of required slope angles makes the bench width variable. The bench width is constant if OSA is kept constant throughout the orebody. However, different bench widths are formed if different OSAs are required to be incorporated in the design. Bench width is calculated by utilizing Eq. (1). Then, positions of the blocks are converted into radii and values of bench width are inserted in Eq. (2). Radius of the pit template on the level where the block is located and radius of the block are calculated by Eqs. (2) and (3), respectively.

$$w = \frac{nb h(\tan \theta - \tan \beta)}{(nb - 1) \tan \theta \tan \beta} \quad (1)$$

$$R = L - \frac{z}{\tan \theta} - w(bl - 1) \quad (2)$$

$$r = \sqrt{x^2 + y^2} \quad (3)$$

where r is distance between a block and the center of the pit, which is determined by SA algorithm; R is the distance between the boundary of the pit and the center of pit; w is bench width; h is bench height; θ is bench slope angle, β is OSA, z is depth of the block from the top of the model; bl is bench level on which the block is located; nb is number of benches, and L is maximum radius of the pit. Equations (1) and (2) are derived from the pit templates similarly generated as the templates shown in Figs. 1, 2 and 4.

If a block is inside the pit contour, then it is considered as selected or extracted. To check whether the block is inside the pit contour, the radius from the center of the pit to the block and the radius of the pit are compared. The center of the pit is determined by SA algorithm. R and r are used to express the following condition: if R is greater than or equal to r , the block is included in the pit; thus, the block is extracted (Fig. 1a). The center of the block is considered when checking whether this condition is satisfied or not. Examples of representative cross sections of cone templates used for different cases or specific situations are shown in Fig. 1. The block height can be the same height as the bench height in the algorithm.

In Fig. 1a, a cross section of a simple template with one bench is shown, in which parameters and variables used in Eqs. (1)–(3) are indicated. The OSA is the same throughout the orebody for this

case. In Fig. 1b, a cross section of the template used for the cases where the OSA is variable in different azimuth ranges is given where β_n and β_{n+1} represent different OSAs and L_n and L_{n+1} represent the corresponding lateral distances. In Fig. 1b, “ n ” is the number of different OSAs, and L_n is the corresponding horizontal distance. “ n ” is an input variable of the algorithm and has no theoretical limit. However, the practical condition of designing pits is expected to be limited also by geotechnical constraints.

In Fig. 1c, tangent of β is equal to the following *Proof-1*:

$$\tan \beta = \frac{4 \cdot h}{3w + \frac{4h}{\tan \theta}}$$

which can be generalized as:

$$\tan \beta = \frac{nb \cdot h}{w(nb - 1) + \frac{nb \cdot h}{\tan \theta}}$$

The following algebraic manipulations enable to obtain the equation of w (bench width):

$$w \cdot (nb - 1) \tan \beta + \frac{nb \cdot h \cdot \tan \beta}{\tan \theta} = nb \cdot h$$

$$w \cdot (nb - 1) \tan \beta = nb \cdot h - \frac{nb \cdot h \cdot \tan \beta}{\tan \theta}$$

$$w \cdot (nb - 1) \tan \beta = nb \cdot h \left(1 - \frac{\tan \beta}{\tan \theta} \right)$$

$$w \cdot (nb - 1) \tan \beta = nb \cdot h \left(\frac{\tan \theta - \tan \beta}{\tan \theta} \right)$$

$$w = \frac{nb \cdot h(\tan \theta - \tan \beta)}{(nb - 1) \tan \theta \tan \beta}$$

which is equal to Eq. (1).

In Fig. 1d, using the parameters indicated, R is found as *Proof-2*:

$$\begin{aligned} R &= L - \frac{h}{\tan \theta} - w - \frac{h}{\tan \theta} - w - \frac{(z - 2h)}{\tan \theta} \\ &= L - \frac{z}{\tan \theta} - 2w \end{aligned}$$

For the block in Fig. 1d, where $bl = 3$ (the block is on the 3rd bench), R is found using Eq. (2) as:

$$R = L - \frac{z}{\tan \theta} - w(bl - 1) = L - \frac{z}{\tan \theta} - 2w$$

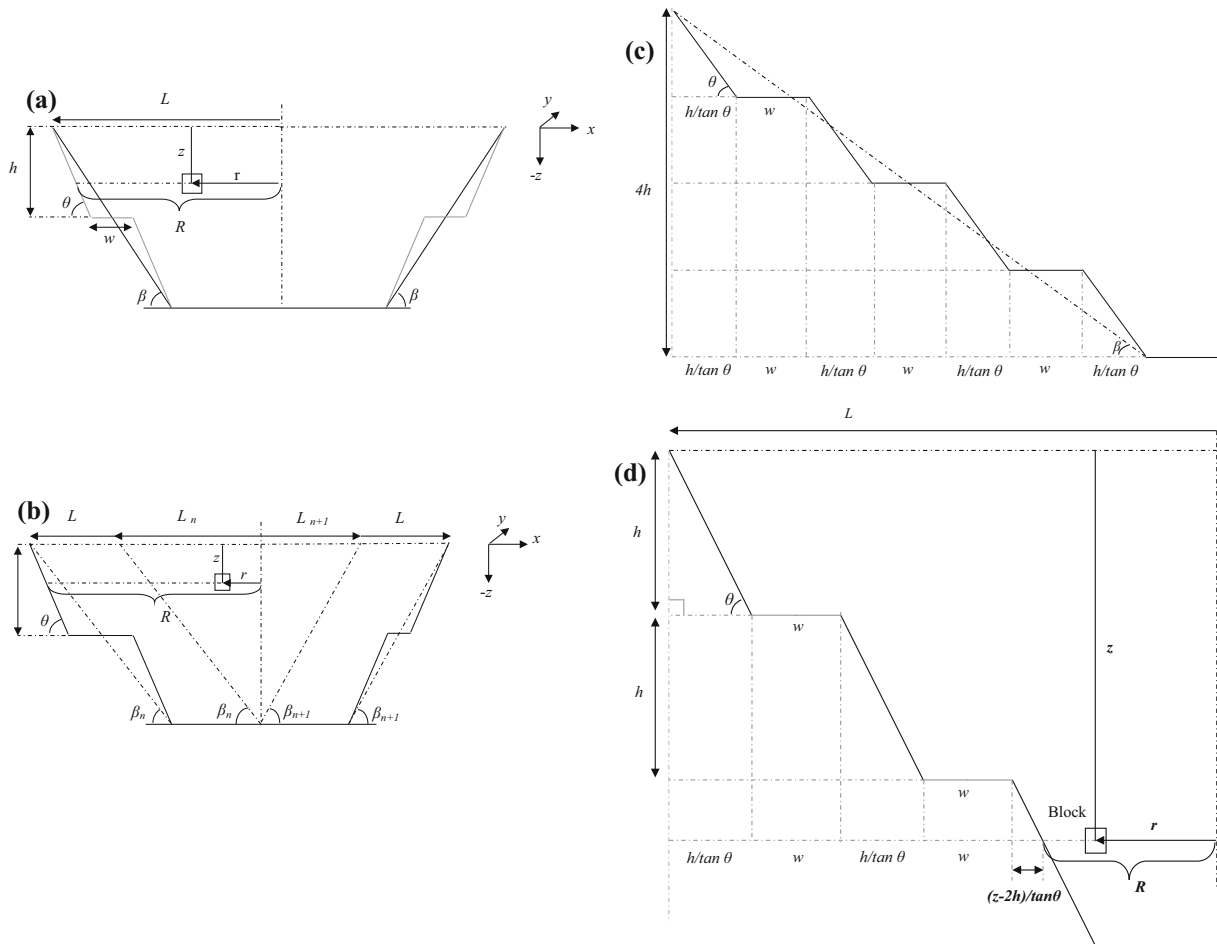


Figure 1. Pit templates in cross-sectional views for **a** constant OSA and **b** variable OSAs changing with respect to azimuth. Pit templates used for **c** proof of Eq. (1) and **d** proof of Eq. (2). “z” represents the depth from an arbitrary block measured from the top level.

Then, L_n (Eq. 11) and H_μ [Eqs. (12) and (13)] are used to generate the mathematical model for MIP. In the cross section given in Fig. 2, the OSA is not the same in different zones with respect to depth. By using the parameters L_t and L_d shown in Fig. 2, Eqs. (10)–(13) are formed for MIP. A mathematical model is also generated for cases where OSA changes with respect to depth and azimuth and the pit template used is similar to the geometry given in Fig. 2.

Mathematical Model for MIP in the Algorithm

MIP was used in the algorithm because there are binary and continuous decision variables in the problem. The objective function consisted of economic block values and binary values of the blocks

[Eq. (4)]. The constraints provided results in accordance with OSAs and ensured restriction on maximum and minimum magnitude of the pit radius [Eqs. (5)–(8)]. The software for solving MIP is a default solver called CBC in PuLP package in Python programming language.

$$\text{Maximize } \sum_{i \in I} \text{BEV}_i b_i \tag{4}$$

subject to

$$\frac{nbh}{\tan \beta} \leq L \leq \max_r + \frac{nbh}{\tan \beta} \tag{5}$$

$$R_i - r_i \geq -M(1 - b_i) \tag{6}$$

$$R_i - r_i \leq M b_i \tag{7}$$

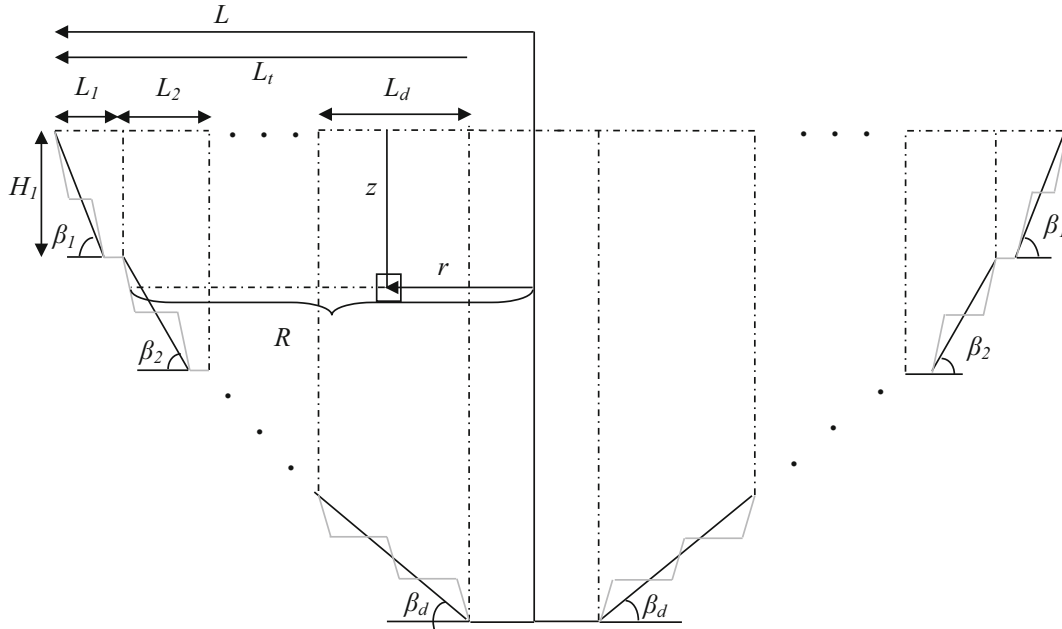


Figure 2. Pit template in cross-sectional view for variable OSAs that change with depth.

$$b_i \in \{0, 1\}, \forall i \in I \tag{8}$$

where BEV_i is economic block value, I is set of all blocks, b_i is binary decision variable, i is block, M is a large constant, and \max_r is maximum of radii of all blocks.

In the defined set of constraints given in Eqs. (6) and (7), any constant number large enough to produce an optimum result can be used for M . These equations were created to implement the following model conditions:

Condition 1 If block b_i is included in the pit, $R_i - r_i$ must be greater than or equal to 0 and b_i is 1.

Condition 2 If block b_i is not included in the pit, $R_i - r_i$ must be less than 0 and b_i is 0.

The main objective function used for constant OSA is given in Eqs. (4)–(8). The equation of R_i depends on the location of the block and variation of OSA. For example, if the OSA changes as the azimuth varies, instead of Eqs. (5) and (2), Eqs. (9) and (11) are used, respectively. If OSA changes in the different ranges of depth, for constraint L and equation R_i , Eqs. (10) and (12) are used, respectively. Equations (9) and (13) are used for cases where the OSA varies with both depth and azimuth. In Fig. 3, the algorithm’s steps at which these equations are used

are shown where “ N ” is defined to be equal to the depth of the block model divided by the bench height, making it a unitless integer value.

$$0 \leq L \leq \max_r \tag{9}$$

$$L_t \leq L \leq \max_r + L_t \tag{10}$$

$$R_i = L + L_n - \frac{z}{\tan \theta} - w_n(bl - 1) \tag{11}$$

$$R_i = L - \sum_{\mu=0}^{D-1} L_\mu - \frac{z - \sum_{\mu=0}^{D-1} H_\mu}{\tan \theta} - w_d(bl_d - 1) \tag{12}$$

$$R_i = L + L_t - \sum_{\mu=0}^{D-1} L_\mu - \frac{z - \sum_{\mu=0}^{D-1} H_\mu}{\tan \theta} - w_{a,d}(bl_d - 1) \tag{13}$$

where bl_d is bench level on which the block is located in one depth range, d is number of ranges of depth, D is order of the depth range from the top of the block model, w_d is bench width in one depth range, w_n is bench width in one azimuth range, $w_{a,d}$ is bench width in one range of azimuth and depth, and L_0 and H_0 are parameters that equal to zero. To

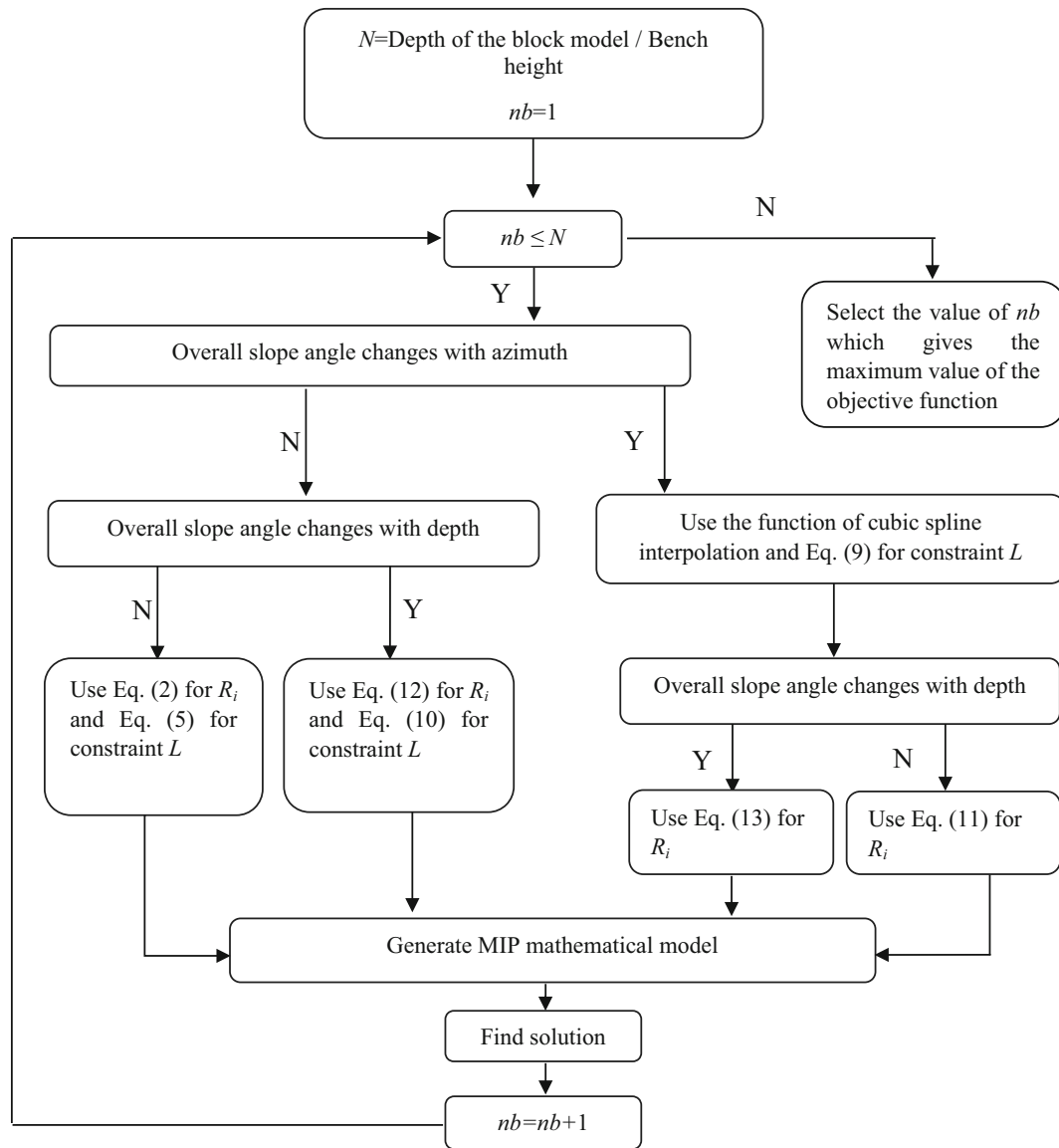


Figure 3. Flowsheet of the optimization algorithm.

explain further the constraints and the *Conditions 1* and 2, the following examples are given. If the equation R_i (Eq. (2)) is substituted in Eqs. (6) and (7), the following inequalities are obtained:

$$L - \frac{z}{\tan \theta} - w(bl - 1) - r_i \geq -M(1 - b_i) \quad (14)$$

$$L - \frac{z}{\tan \theta} - w(bl - 1) - r_i \leq M b_i \quad (15)$$

For parameters $nb = 4$, $\theta = 60^\circ$, and $\beta = 45^\circ$, w is found as 5.635 m by using Eq. (1). Then, $w = 5.635$,

$bl = 3$, $z = 25$, $\theta = 60^\circ$, $M = 10,000$, $r_i = 50$ m are substituted in Eqs. (14) and (15). For the block b_i , the constraints will be as follows:

$$L - 75.704 \geq -10,000(1 - b_i) \quad (16)$$

$$L - 75.704 \leq 10,000b_i \quad (17)$$

If L is equal to 150 at the end of the optimization process, then Eqs. (16) and (17) will become, respectively, as:

$$74.296 \geq -10,000(1 - b_i) \quad (18)$$

$$74.296 \leq 10,000b_i \quad (19)$$

- For $b_i = 0$, the constraint [Eq. (17)] will not be satisfied:

$$74.296 \geq -10,000$$

$$74.296 \leq 0$$

- For $b_i = 1$, the constraints [Eqs. (16) and (17)] will be satisfied:

$$74.296 \geq 0$$

$$74.296 \leq 10,000$$

Thus, if L is equal to 150 m, for this specific block, b_i is 1. If L is equal to 10 at the end of the optimization procedure, the constraints will be as follows:

$$-65.704 \geq -10,000(1 - b_i) \quad (20)$$

$$-65.704 \leq 10,000b_i \quad (21)$$

- For $b_i = 0$, the constraints [Eqs. (20) and (21)] will be satisfied:

$$-65.704 \geq -10,000$$

$$-65.704 \leq 0$$

- For $b_i = 1$, the constraint [Eq. (20)] will not be satisfied:

$$-65.704 \geq 0$$

$$-65.704 \leq 10,000$$

Thus, if L is equal to 10 m, for this specific block, b_i is 0.

SA in the Algorithm

The SA algorithm was used to decrease the solution time in the proposed algorithm. The center of the pit, which gives the maximum profit, was determined from the solutions generated by the SA algorithm. After a solution was found, the ultimate pit limit problem was solved with MIP to achieve the exact solution. The main steps of the SA algorithm modified for the open pit problem are given in Algorithm 2.

Neighborhood solutions were created with consideration of pit geometry constraints (bench height, bench slope, OSA). The constraints were similar to the ones in the MIP problem. However, the equations were changed so that they can be suitable for the SA algorithm. The starting temper-

ature was chosen as 10^6 so that the probability of accepting a worse move was initially high. According to the SA theory, the final temperature was equal to 0 (Talbi, 2009). For this reason, the finishing temperature was selected as 1.87×10^{-8} so that it can be close to 0 as much as possible. The number of neighborhood solutions was 60. These parameters were problem-specific, and multiple trials must be carried out to determine the right parameters for reaching an optimum solution.

The parameter alpha, representing the temperature decreasing constant, was selected as 0.9 in the algorithm because it is suggested to be between 0.50 and 0.99 (Aarts & Laarhoven, 1987). This value generates various inputs of the temperature changing from the highest to the lowest, and at each value of the temperature, the x and y coordinates of the center of the pit are randomly chosen from the set of integer numbers. With the coordinates, the pit contour was formed without violating the slope constraints, and neighborhood solutions were obtained; the pit size increased or decreased depending on the acceptance criteria.

Cubic Spline Interpolation in the Algorithm

In the algorithm, cubic spline interpolation was used for two cases in which OSA changes with respect to azimuth. Cubic spline interpolation provides smoother pit shapes by converting angles into points. A curve between the points is created by the interpolation. Then, the points on the curve were converted into azimuth and OSAs. The detailed steps of the cubic spline interpolation for variable slope angles were as follows (Sattarvand & Shisvan, 2012):

- Slope angles and azimuth were converted into points of x and y coordinates by using Eqs. (22) and (23), which were obtained by geometrical relationships and demonstrated in Fig. 4.
- Polynomial functions of a variable t [Eq. (25)] were created for both x and y coordinates with points obtained in the previous step. “ t ” was the variable of the polynomial function of a curve segment. By substituting x and y coordinates into the right-hand side of Eq. (24), P_k^t values were found for x and y separately. Then, P_k (x and y coordinates) and P_k^t values are substituted

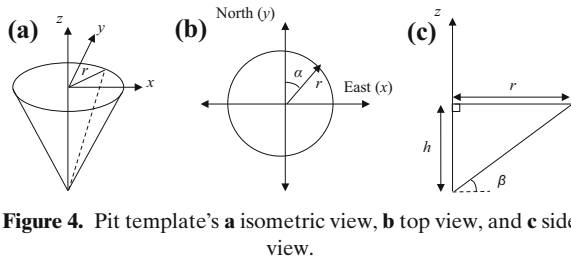


Figure 4. Pit template's **a** isometric view, **b** top view, and **c** side view.

into Eq. (25). For k points given, $(k - 1)$ number of polynomial functions for x and $(k - 1)$ number of polynomial functions for y were obtained. Equations (24) and (25) are provided in the paper published by Sattarvand & Shisvan, 2012, and further explanation is given by Salomon (2006).

- Values incremented by 0.1 in the range of 0 and 1 were given to the parameter t for all polynomial functions in order to determine a set of points on the curve segment.
- Cubic spline interpolation was performed on each horizontal level. Points on the curve on each level were obtained, and the corresponding OSAs are used for Eqs. (11) and (13).

$$x = \frac{h}{\tan \beta \sqrt{1 + \cot^2 \alpha}} \tag{22}$$

$$y = x \cot \alpha \tag{23}$$

where α is azimuth

$$\begin{bmatrix} 1 & 4 & 1 & \dots & 0 & \dots & 0 \\ 0 & 1 & 4 & 1 & \dots & \dots & 0 \\ & & & \ddots & \ddots & & \\ 0 & \dots & \dots & \dots & 1 & 4 & 1 \\ 1 & \dots & \dots & \dots & 0 & 1 & 4 \\ 4 & 1 & 0 & \dots & 0 & 0 & 1 \end{bmatrix}_{(n \times n)} \begin{bmatrix} P_1^t \\ P_2^t \\ P_3^t \\ \vdots \\ P_{n-1}^t \\ P_n^t \end{bmatrix} = \begin{bmatrix} 3(P_3 - P_1) \\ 3(P_4 - P_2) \\ \vdots \\ 3(P_{n+1} - P_{n-1}) \\ 3(P_{n+2} - P_n) \end{bmatrix} \tag{24}$$

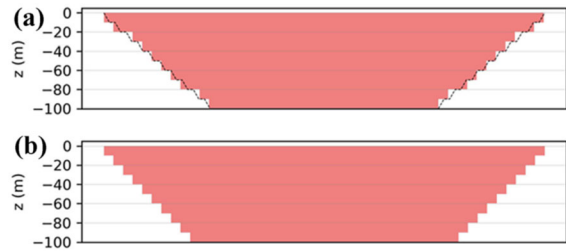


Figure 5. Cross sections of extracted blocks generated by **a** the proposed algorithm and **b** the LG algorithm.

Table 1. Comparison of MIP and LG algorithm

Scenario	# of Extracted blocks		Improvement in solution (%)
	LG	MIP	MIP
1	295,240	324,588	10.0
2		321,030	8.7
3		353,300	19.7
4		317,574	7.5

$$P(t) = P_k + P_k^t \cdot t + (3(P_{k+1} - P_k) - 2P_k^t - P_{k+1}^t) \cdot t^2 + (2(P_k - P_{k+1}) + P_k^t + P_{k+1}^t) \cdot t^3 \tag{25}$$

The mathematical model, SA, and cubic spline interpolation components of the algorithm were validated for different case studies representing various surface mining operations.

RESULTS AND DISCUSSION

The ultimate pit limit problem of a block model with cubic blocks was solved with the proposed algorithm and the LG algorithm to demonstrate the difference between pit contours. The proposed algorithm was also implemented on case studies with different number of blocks. An optimal solution of the MIP problem was reached in approximately 90, 350, 410, and 730 s when the algorithm was applied to block models with 81,600, 107,916 and 118,096 blocks. In these block models, block dimensions were 10 m, 10 m, and 2 m in x , y , and z directions, respectively. Block dimensions of 10 m, 10 m, 2 m were used to investigate the accuracy of the algorithm by following the desired slope angle in detail.

Economic Block Value Parameters

Price	<input type="text" value="20"/>
Selling cost	<input type="text" value="0.5"/>
Mining cost	<input type="text" value="1"/>
Processing cost	<input type="text" value="1"/>
Average density	<input type="text" value="3.5"/>
Mining cost increase per meter of depth	<input type="text" value="0.05"/>
Recovery	<input type="text" value="100"/>

Bench Parameters

Bench height	<input type="text" value="10"/>
Bench face angle	<input type="text" value="60"/>

Choose One of the Cases:

- Constant overall slope angle
- Overall slope change with respect to azimuth
- Overall slope change with respect to depth
- Overall slope change with respect to depth and azimuth

3D Figures

- Display the final pit
- Display the extracted blocks

Figure 6. Input window for the economic block value parameters, the bench parameters, and the selection of OSA.

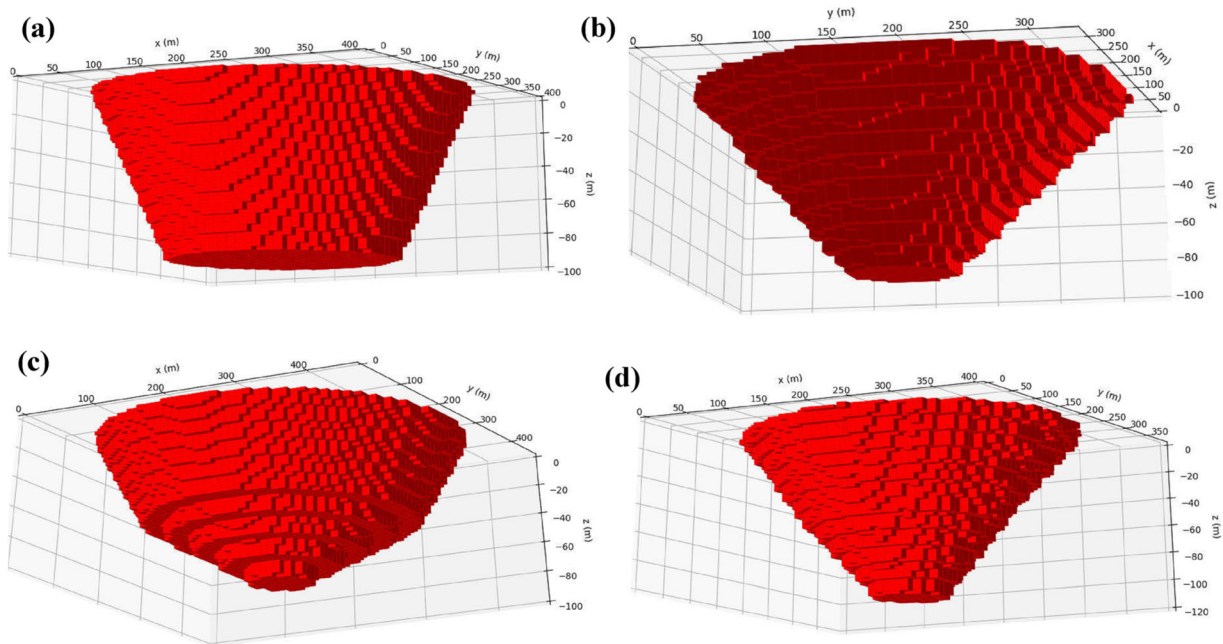


Figure 7. Extracted blocks for Case Study 1 (a), 2 (b), 3 (c), and 4 (d).

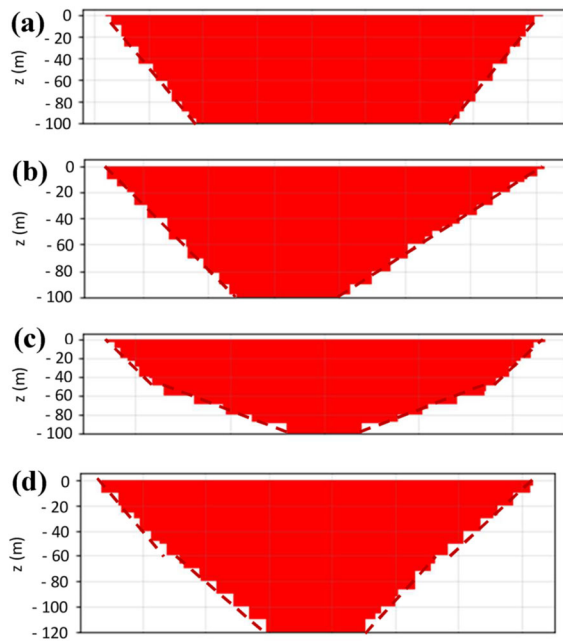


Figure 8. N 40° E cross sections of the extracted blocks for Case Study 1 (a), 2 (b), 3 (c), and 4 (d).

Table 3. OSAs in different azimuth ranges (Case Study 2)

OSA (°)	Azimuth range (°)
35	0–20
33	35–45
37	100–120
40	150–160
43	160–180
45	215–225
40	265–285
36	330–350

on four scenarios. Scenario-1 was defined for a constant slope angle, and Scenario-2 was defined for the slope angle changed for different azimuth values. Scenario-3 was the variance of slope angle with depth levels, and Scenario-4 was the implementation of slope angle changes according to azimuth values and depth levels together. Because the generated slope angles depend on the block dimensions in LG algorithm, only one pit shape with 45° and 35.26° slopes in two cross sections was formed. With the

Table 2. Comparison of OSAs (Case Study 1 and Case Study 2)

	Cross section	Input value (°)	Measured value (°)	Difference (°)	Input value (°)	Measured value (°)	Difference (°)
Case Study 1	N–S	51	51.340	0.340	51	51.340	0.340
Case Study 2	N 40 E	33	32.604	0.396	45	45.007	0.007
	S 25 W	40	38.773	1.227	36	34.883	1.117

OSAs that were used as inputs were compared to the measured OSAs obtained from the results in order to check the validity of the proposed mathematical model and algorithm. In addition, the solutions of the pit with variable and uniform slope angles were compared as the final limit of a pit will be different if a conventional method such as LG algorithm was used (Fig. 5).

The cross sections of extracted blocks generated by LG and the proposed algorithm (Fig. 5) were different, as the contour of the pit geometry was formed including bench width and bench height in the proposed algorithm. The pit contour consisting of 60° bench slope and about 6-m bench width created a different pit contour. The proposed algorithm was compared with the LG algorithm using a block model with 1,238,400 cubic blocks. MIP was applied

proposed method, steeper angles between 55° and 58° can be formed, and the proposed algorithm generated more profitable pits than the LG algorithm (Table 1). The result of the proposed algorithm was more profitable, as the constraints that were defined for specific problems were different. The constraints used for LG were different from those of the proposed algorithm. With MIP, a steeper slope can be achieved without the influence of block dimensions; in the LG method, a lower slope angle can only be formed by changing the block dimensions. Thus, in some cases, this algorithm can still provide better results, especially for cases where slope angles are varied for different bearing angles or different depth levels, as preferred commonly within the life time of the mine.

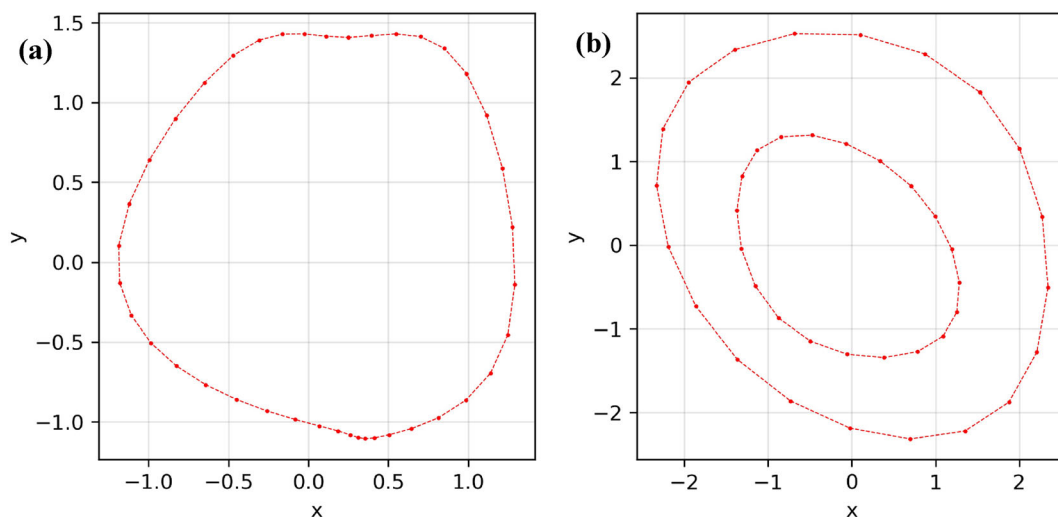


Figure 9. Curves created by cubic spline interpolation for (a) Case Study 2 and (b) Case Study 4.

Table 4. Comparison of OSAs (Case Study 3 and Case Study 4)

	Cross sections	Depth range (m)	OSA					
			Input value (°)	Measured value (°)	Difference (°)	Input value (°)	Measured value (°)	Difference (°)
Case Study 3	N 45 E	0–50	45	49.684	4.684	45	49.684	4.684
		50–100	20	21.447	1.447	20	21.447	1.447
	W–E	0–50	45	45.000	0	45	45.000	0
		50–100	20	21.038	1.038	20	21.038	1.038
Case Study 4	N 45 E	0–60	40	40.316	0.316	46	46.686	0.686
		60–120	45	46.686	1.686	39	40.316	1.316
	S 45 E	0–60	37	35.264	1.736	36	40.316	4.316
		60–120	33	31.220	1.780	32	31.220	0.780

Table 5. OSA in different azimuth and depth ranges (Case Study 4)

Depth range (m)	OSA (°)	Azimuth range (°)
0–60	40	0–80
	37	100–170
	46	190–260
	36	280–350
60–120	45	0–90
	33	90–180
	39	180–270
	32	270–360

The parameters required for the optimization are entered in the graphical user interface (GUI) as

shown in Fig. 6. The economic block value and the bench parameters are the same for all cases. Bench height and bench face angle are entered as 10 m and 60°, respectively. Four choices of overall slope change are available in the GUI given in Fig. 6.

For Case Study 1, the OSA of 51° was defined as constant, and so spline interpolation was not used for this condition. The extracted blocks and a sample cross section are shown in Figs. 7a and 8a. In these figures, OSA is constant, and the measured slope angles obtained from the result of the optimization were compared to the angle. The difference between OSA taken from input and output data was 0.340° on N–S and W–E cross sections in Case Study 1 (Table 2).

Table 6. Comparison of case studies in SA runs

Case study	# of blocks (size of the block model)	Average difference of angles (°)	Solution time (s)
1	81,600	0.340	732.6
2	81,600	0.687	91.8
3	107,916	1.792	348.0
4	118,096	1.577	411.8

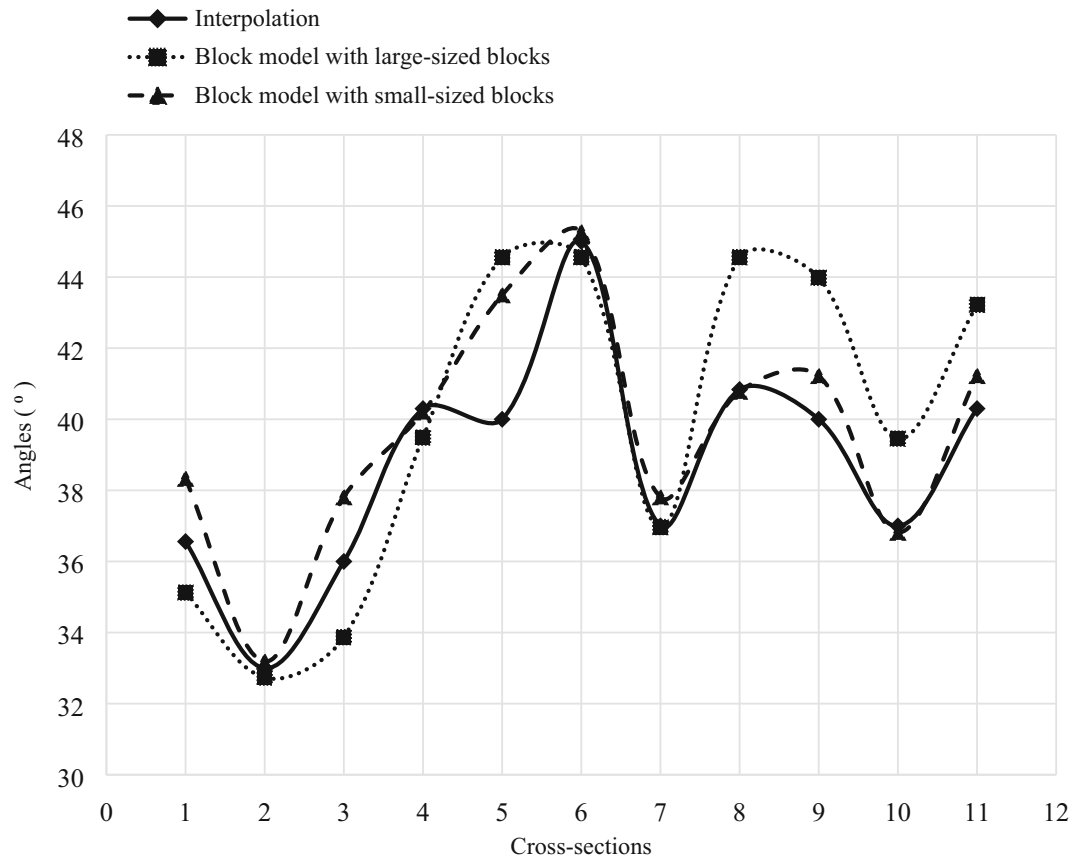


Figure 10. Comparison between input and output values of OSA of the block models with large-sized and small-sized blocks.

For the cross sections given in Table 2, the average difference between OSAs taken from input and output data was 0.687° for Case Study 2. The second example was provided to check the validity of the algorithm for the case in which OSA changes with respect to azimuth and spline interpolation is used. Number of zones entered as 8 in the GUI are given in Table 3, although any number of zones can be entered in the algorithm. The plan view of the pit template for a unit height created by spline inter-

polation and the extracted blocks for Case Study 2 are shown in Figs. 9a and 7b, respectively. It can be seen that OSA was not constant with respect to azimuth in Figs. 7b and 8b.

The algorithm was applied to Case Study 3, in which OSA variation with depth was evaluated without using spline interpolation. Different OSA values were entered for the two zones with depths of 0–50 m and 50–100 m and slope angles of 45° and 20°, respectively. The slope angle of 20° was used to

show the accuracy of the algorithm to follow the abrupt slope change as the depth increases. Although a geotechnical analysis was not performed within the scope of this study, it might be the case that a discontinuity set or any other weakness plane might limit the pit geometry to reduce the slope angles according to the orientation and strength parameters of the discontinuity. Extracted blocks are shown in Fig. 7c, and a cross section is shown in Fig. 8c where the two different zones based on depth can be identified distinctly at about 50 m. For Case Study 3, the average difference between OSA taken from input and output data was 1.792° (Table 4).

Case Study 4 was a scenario where OSA changes with respect to both depth and azimuth. Spline interpolation was used to generate the angles for this case, and eight different OSA were entered in the GUI for two zones of depth and four zones of azimuth (Table 5). One of the spline curves was used for depth range of 0–60 m, and the other one was utilized for depth range of 60–120 m. Extracted blocks in Case Study 4 are shown in Fig. 7d, and the varying OSA with respect to azimuth is shown in Fig. 8d. The change in slope angle with respect to depth in Fig. 7d is not as apparent as it is in Fig. 7c because the difference between angles for the two depth ranges was 25° for the extracted blocks in Fig. 7c and $4\text{--}7^\circ$ for the extracted blocks in Fig. 7d. The SA algorithm was run for 30 times to determine center of the pit bottom prior to MIP, and the results for each case were evaluated to select the highest value. The results given in Table 6 summarize the solutions of the case studies.

The pit shape generated by the algorithm becomes more accurate and similar to the actual pit shape with the desired OSA as the number of blocks increases or block dimension decreases. This was evaluated by Case Study 2 compared to another example with the same input but smaller-sized blocks. The economical parameters for these two cases were different from those in the other cases. In Fig. 10, OSAs calculated by interpolation and measured angles from the extracted blocks are given. The average differences of OSA were 0.985° and 2.190° for the models with small-sized and large-sized blocks, respectively, and the small-sized block model had a better conformance to the angle generated by interpolation (Fig. 10).

CONCLUSIONS

The proposed algorithm coded in Python programming language was applied on block models consisting of 81,600; 107,916; 118,096, and 494,900 blocks to verify the mathematical model. The input data for OSA based on geotechnical studies are compared to OSA obtained from the optimization as output data. It was found that the angles are either same or close to each other within a range of 0° to 4.9° . However, the difference between required angles and generated angles by the algorithm becomes smaller as the number of the blocks increases. It can be concluded that the proposed algorithm can be a useful option for incorporation of various OSA into the optimization of the ultimate pit limit. The main advantage of the proposed algorithm is that the pit shape with desired OSA and maximum economic value is simultaneously obtained. A comparison with LG algorithm for different case studies indicated that an improvement within a range of 8–20% could be achieved by means of economic value. The pit layout with the required OSA is not formed after the optimization is finished, and the resultant pit values are greater for the pit contour with variable OSA. Some aspects can be considered so that the proposed approach can be improved further. It is planned to incorporate the topography for a more realistic design, whereas geotechnical aspects are also planned to be defined as constraints of the solution in the algorithm.

REFERENCES

- Aarts, E. H. L., & Van Laarhoven, R. J. (1987). *Simulated annealing: Theory and applications*. Reidel.
- Achireko, P. K. (1998). *Application of modified conditional simulation and artificial neural networks to open pit optimization*. Technical University of Nova Scotia.
- Albor Consuegra, F. R., & Dimitrakopoulos, R. (2009). Stochastic mine design optimisation based on simulated annealing: Pit limits, production schedules, multiple orebody scenarios and sensitivity analysis. *Mining Technology*, 118(2), 79–90.
- Askari-Nasab, H., Pourrahimian, Y., Ben-Awuah, E., & Kalantari, S. (2011). Mixed integer linear programming formulations for open pit production scheduling. *Journal of Mining Science*, 47(3), 338–359.
- Bai, V. X., Turczynski, G., Baxter, N., Place, D., Sinclair-Ross, H., & Ready, S. (2017). Pseudoflow method for pit optimization. Whitepaper, Geovia-Whittle, Dassault Systems.
- Barnes, R. J., & Johnson, T. B. (1982). Bounding techniques for the ultimate pit limit problem. In *Proc. 17th APCOM* (pp. 263–273). AIME.

- Blom, M., Pearce, A. R., & Stuckey, P. J. (2017). Short-term scheduling of an open-pit mine with multiple objectives. *Engineering Optimization*, 49(5), 777–795.
- Blom, M., Pearce, A. R., & Stuckey, P. J. (2018). Multi-objective short-term production scheduling for open-pit mines: A hierarchical decomposition-based algorithm. *Engineering Optimization*, 50(12), 2143–2160.
- Campos, P. H. A., Arroyo, C. E., & Morales, N. (2018). Application of optimized models through direct block scheduling in traditional mine planning. *The Journal of the Southern African Institute of Mining and Metallurgy*, 118, 381–386.
- Cerny, V. A. (1985). Thermodynamical approach to the traveling salesman problem: An efficient simulation algorithm. *Journal of Optimization Theory and Applications*, 45, 41–51.
- Chaves, L. S., Carvalho, L. A., Souza, F. R., Nader, B., Ortiz, C. E. A., Torres, V. F. N., Câmara, T. R., Napa-García, G. F., & Valadão, G. E. S. (2020). Analysis of the impacts of slope angle variation on slope stability and NPV via two different final pit definition techniques. *REM - International Engineering Journal*, 73(1), 119–126.
- Chen, T. (1976). 3D pit design with variable wall slope capabilities. In *Proc. 14th APCOM* (pp. 615–625). AIME.
- CIM. (2019). CIM Estimation of Mineral Resources and Mineral Reserves Best Practice Guidelines. Retrieved April 21, 2021, from https://www.bsc.bc.ca/-/media/PWS/Resources/For_Companies/Mining/CIM-Best-Practices-Guidelines-November-29-2019.pdf.
- Dagasan, Y., Renard, P., Straubhaar, J., Erten, O., & Topal, E. (2019). Pilot point optimization of mining boundaries for lateritic metal deposits: Finding the trade-off between dilution and ore loss. *Natural Resources Research*, 28, 153–171.
- Dekkers, A., & Aarts, E. (1991). Global optimization and simulated annealing. *Mathematical Programming*, 50, 367–393.
- Deutsch, M., González, E., & Williams, M. (2015). Using simulation to quantify uncertainty in ultimate-pit limits and inform infrastructure placement. *Mining Engineering*, 67(12), 49–55.
- Dowd, P., & Onur, A. H. (1993). Open pit optimization—part 1: Optimal open pit design. *Trans. Instn Min Metall (Sect. A: Min. industry)*, 102, A95–A104.
- Elahi, E., Kakaie, R., & Yousefi, A. (2011). A new algorithm for optimum open pit design: Floating cone method III. *Journal of Mining & Environment*, 2(2), 118–125. <https://doi.org/10.22044/JME.2012.63>.
- Farmer, I., & Dimitrakopoulos, R. (2018). Schedule-based push-back design within the stochastic optimisation framework. *International Journal of Mining, Reclamation and Environment*, 32(5), 327–340.
- Fu, Z., Asad, M. W. A., & Topal, E. (2019). A new model for open-pit production and waste-dump scheduling. *Engineering Optimization*, 51(4), 718–732.
- Giannini, L. M. (1990). *Optimum design of open pit mines*. Curtin University of Technology.
- Gilani, S. O., & Sattarvand, J. (2015). A new heuristic non-linear approach for modeling the variable slope angles in open pit mine planning algorithms. *Acta Montanistica Slovaca*, 20(4), 251–259.
- Hochbaum, D. S., & Chen, A. (2000). Performance analysis and best implementations of old and new algorithms for the open pit mining problem. *Operation Research*, 48(6), 894–914.
- Hochbaum, D. S. (2008). The pseudoflow algorithm: A new algorithm for the maximum-flow problem. *Operations Research*, 56(4), 992–1009. <https://doi.org/10.1287/opre.1080.0524>.
- Huttagosol, P. (1988). Modified tree graph algorithm for ultimate pit limit analysis. MSc diss., Colorado School of Mines.
- Jalali, S. E., Ataee-Pour, M., & Shahriar, K. (2006). Pit limit optimization using stochastic process. *CIM Bulletin*, 99(1024), 1–11.
- Javadzadeh, S., Ataee-pour, M., & Hosseinpour, V. (2019). Modeling optimum mining limits with imperialist competitive algorithm. In *Proceedings of the 27th international symposium on mine planning and equipment selection-MPES 2018* (pp. 197–211). Springer.
- Johnson, T. B. (1968). *Optimum open pit mine production scheduling*. California University, Berkeley, Operations Research Center.
- Johnson, T. B., & Sharp, W. R. (1971). A three-dimensional dynamic programming method for optimal ultimate open pit design. *USBM*, 7553(25).
- Khalokakaie, R. (1999). *Computer-aided optimal open pit design with variable slope angles*. University of Leeds.
- Khalokakaie, R. (2006). Optimum open pit design with modified moving cone II methods. *Journal of Engineering in Tehran University*, 41(3), 297–307. (In Persian).
- Kirkpatrick, S., Gelatt, C. D., & Vecchi, M. P. (1983). Optimization by simulated annealing. *Science*, 220(4598), 671–680.
- Koenigsberg, E. (1982). The optimum contours of an open pit mine: an application of dynamic programming. In *Proc. 17th APCOM* (pp. 274–287). AIME.
- Kumral, M., & Dowd, P. A. (2004). A simulated annealing approach to mine production scheduling. *Journal of the Operational Research Society*, 56(8), 922–930.
- Kumral, M. (2012). Production planning of mines: Optimisation of block sequencing and destination. *International Journal of Mining, Reclamation and Environment*, 26(2), 93–103. <http://doi.org/10.1080/17480930.2011.644474>.
- Kumral, M. (2013). Optimizing ore-waste discrimination and block sequencing through simulated annealing. *Applied Soft Computing*, 13(8), 3737–3744. <https://doi.org/10.1016/j.asoc.2013.03.005>.
- Lerchs, H., & Grossmann, I. F. (1965). Optimum design of open pit mines. *CIM Bulletin*, 58, 47–54.
- L'Heureux, G., Gamache, M., & Soumis, F. (2013). Mixed integer programming model for short term planning in open-pit mines. *Mining Technology*, 122(2), 101–109.
- Li, S., Sari, Y. A., & Kumral, M. (2020). Optimization of Mining-Mineral Processing Integration Using Unsupervised Machine Learning Algorithms. *Natural Resources Research*, 29, 3035–3046. <https://doi.org/10.1007/s11053-020-09628-0>.
- Lipkewich, M. P., & Borgman, L. (1969). *Two- and three-dimensional pit design optimization techniques* (pp. 505–523). A Decade of Digital Computing in the Mineral Industry. AIME.
- Locatelli, M. (2000). Simulated annealing algorithms for continuous global optimization: Convergence conditions. *Journal of Optimization Theory and Applications*, 104, 121–133.
- Madowe, A. (2016). Design and implementation of steeper slope angles on a kimberlite open pit diamond operation—a practical approach. *The Journal of the Southern African Institute of Mining and Metallurgy*, 116, 723–730.
- Malli, T., Pamukcu, C., & Kose, H. (2015). Determination of optimum production capacity and mine life considering net present value in open pit mining at different overall slope angles. *Acta Montanistica Slovaca*, 20(1), 62–70.
- Meyer, M. (1969). Applying linear programming to the design of ultimate pit limits. *Management Science*, 16(2), B121–B135.
- Metropolis, N., Rosenbluth, A., Rosenbluth, M., Teller, A., & Teller, E. (1953). Equation of state calculations by fast computing machines. *Journal of Chemical Physics*, 21, 1087–1092.
- Milani, G. A. (2016). Genetic algorithm with zooming for the determination of the optimal open pit mines layout. *The Open Civil Engineering Journal*, 10, 301–322.
- Mousavi, A., Kozan, E., & Liu, S. Q. (2016). Open-pit block sequencing optimization: A mathematical model and solution technique. *Engineering Optimization*, 48(11), 1932–1950.

- Osanloo, M., Gholamnejad, J., & Karimi, B. (2008). Long-term open pit mine production planning: A review of models and algorithms. *International Journal of Mining, Reclamation and Environment*, 22(1), 3–35.
- Ozdamar, L., & Demirhan, M. (2000). Experiments with new stochastic global optimization search techniques. *Computers and Operations Research*, 27(9), 841–865.
- Pana, M. T. (1965). The simulation approach to open pit design. In *Proc. 5th APCOM* (pp. 1–24). University of Arizona, Tucson, Arizona, USA.
- Parra, A., Morales, N., Vallejos, J., & Nguyen, P. M. V. (2018). Open pit mine planning considering geomechanical constraints. *International Journal of Mining, Reclamation and Environment*, 32(4), 221–238.
- Picard, J. C. (1976). Maximum closure of a graph and applications to combinatorial problems. *Management Science*, 22(11), 1268–1272.
- Poniewierski, J. (2018). Pseudoflow explained. Deswik, A discussion of Deswik pseudoflow pit optimization in comparison to Whittle LG pit optimization.
- Ramazan, S., & Dimitrakopoulos, R. (2004). Recent applications of operations research and efficient MIP formulations in open pit mining. *Mining, Metallurgy, and Exploration Transactions*, 316, 73–78.
- Rychkun, E., & Chen, T. (1979). Open pit mine feasibility method and application at placer development. In A. Weiss (Ed.), *Computer methods for the 80's in the Mineral Industry* (pp. 304–309). AIME.
- Salomon, D. (2006). Curves and surfaces for computer graphics. *Springer Science & Business Media*. <https://doi.org/10.1007/0-387-28452-4>.
- Sattarvand, J., & Shisvan, M. S. (2012). Modelling of accurate variable slope angles in open-pit mine design using spline interpolation. *Archives of Mining Sciences*, 57(4), 921–932.
- Sayadi, A. R., Fathianpour, N., & Mousavi, A. (2011). Open pit optimization in 3D using a new artificial neural network. *Archives of Mining Sciences*, 56(3), 389–403.
- Shenggui, Z., & Starfield, A. M. (1985). Dynamic programming with colour graphics smoothing for open pit design on a personal computer. *Geotechnical and Geological Engineering*, 3(1), 27–34. <https://doi.org/10.1007/BF00881339>.
- Soltani Khaboushan, A., & Osanloo, M. (2020). A set of classified integer programming (IP) models for optimum transition from open pit to underground mining methods. *Natural Resources Research*, 29, 1543–1559.
- Souza, F. R., Burgarelli, H. R., Nader, A. S., Ortiz, C. E. A., Chaves, L. S., Carvalho, L. A., Torres, V. F. N., Camara, T. R., & Galery, R. (2018). Direct block scheduling technology: Analysis of avidity. *REM - International Engineering Journal*, 71(1), 97–104.
- Stuart, N. J. (1992). Pit optimisation using solid modelling and the Lerchs Grossman algorithm. *International Journal of Surface Mining and Reclamation*, 6(1), 19–29.
- Talbi, E. (2009). *Metaheuristics: From design to implementation*. John Wiley & Sons Inc.
- Wilke, F. L., & Wright, E. A. (1984). Determining the optimal ultimate pit design for hard rock open pit mines using dynamic programming. *Erzmetall*, 37, 139–144.
- Wright, E. A. (1999). Moving Cone II—a simple algorithm for optimum pit limits design. In *Proc. 28th APCOM, Colorado* (pp. 367–374).
- Zhao, Y., & Kim, Y. C. (1992). A new optimum pit limit design algorithm. In *Proc. 23th APCOM* (pp. 423–434).